

Self-Supervised Depth Learning for Urban Scene Understanding

Huaizu Jiang¹, Erik Learned-Miller¹

Gustav Larsson², Michael Maire³, Greg Shakhnarovich³

¹UMass Amherst ²University of Chicago ³TTI-Chicago

{hzjiang, elm}@cs.umass.edu, larsson@cs.uchicago.edu, {mmaire, greg}@ttic.edu

Abstract

As an agent moves through the world, the apparent motion of scene elements is (usually) inversely proportional to their depth.¹ It is natural for a learning agent to associate image patterns with the magnitude of their displacement over time: as the agent moves, far away mountains don't move much; nearby trees move a lot. This natural relationship between the appearance of objects and their motion is a rich source of information about the world. In this work, we train a deep network, using fully automatic supervision, to predict relative scene depth from single images. The depth training images are automatically derived from simple videos of cars moving through a scene, using classic depth from motion techniques, and no human-provided labels. We show that this pretext task of predicting depth from a single image induces features in the network that result in large improvements in a set of downstream tasks including semantic segmentation, joint road segmentation and car detection, and monocular (absolute) depth estimation, over a network trained from scratch. In particular, our pre-trained model outperforms an ImageNet counterpart for the monocular depth estimation task. Unlike work that analyzes video paired with additional information about direction of motion, our agent learns from "raw egomotion" video recorded from cars moving through the world. Unlike methods that require videos of moving objects, we neither depend on, nor are disrupted by, moving objects in the video. Indeed, we can benefit from predicting depth in the videos associated with various downstream tasks, showing that we can adapt to new scenes in an unsupervised manner to improve performance. By doing so, we achieve consistently better results over several different urban scene understanding tasks, obtaining results that are competitive with state-of-the-art method for monocular depth estimation.

¹Strictly speaking, this statement is true only after one has compensated for camera rotation, individual object motion, and image position. We address these issues in the paper.

1. Introduction

How does a newborn agent learn about the world? When an animal (or robot) moves, its visual system is exposed to a shower of information. Usually, the speed with which something moves in the image is inversely proportional to its depth.¹ As an agent continues to experience visual stimuli under its own motion, it is natural for it to form associations between the appearance of objects and their relative motion in the image. For example, an agent may learn that objects that look like mountains typically don't move in the image (or change appearance much) as the agent moves. Objects like nearby cars and people, however, appear to move rapidly in the image as the agent changes position relative to them. This continuous pairing of images with motion acts as a kind of "automatic" supervision that could eventually allow an agent both to understand the depth of objects and to group pixels into objects by this predicted depth. That is, by moving through the world, an agent may gather training data sufficient for learning to understand static scenes.

In this paper, we explore the relationship between the appearance of objects and their relative depth in the image. To estimate object depths without human supervision, we use traditional techniques for estimating depth from motion, applied to simple videos taken from cars. Since these depth estimation techniques produce depth *up to an unknown scale factor*, we output estimates of *relative depth*, where each pixel's value is in the range of $[0, 1]$ denoting its percentile over the entire image. Once we have depth estimates for these video images, we train a deep network to predict the depth of each pixel from a *single image*, i.e., to predict the depth *without* the benefit of motion. One might expect such a network to learn that an image patch that looks like a house and spans 20 pixels of an image is about 100 meters away, while a pedestrian that spans 100 image pixels is perhaps 10 meters away. Figure 1 illustrates this prediction task and shows example results obtained using a standard convolutional neural network (CNN) in this setting. For example, in the leftmost image of Fig. 1, an otherwise unremarkable traffic-light pole is clearly highlighted by its depth

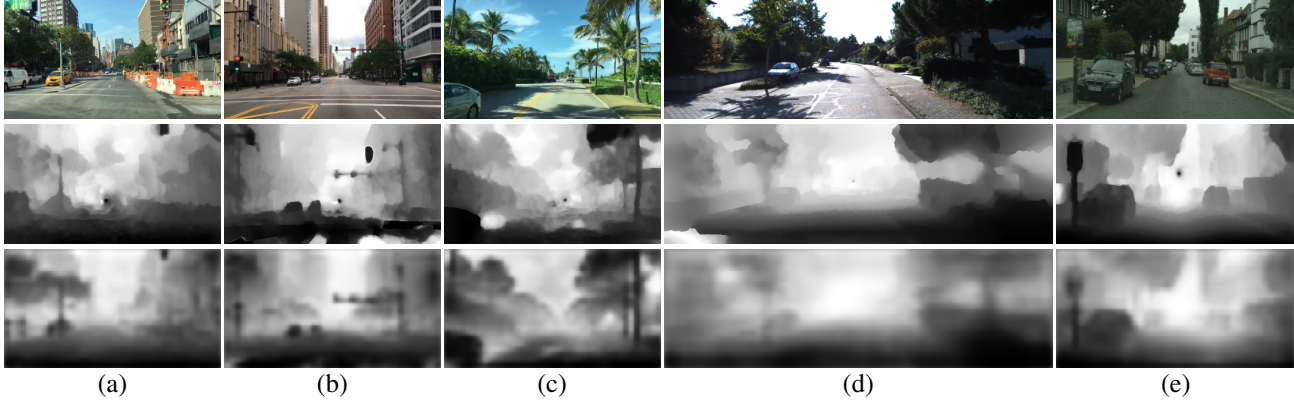


Figure 1: Sample frames from collected videos and their corresponding depth maps, where brightness encodes relative depth. From top to bottom: input image, relative depth image computed using Eq.(3), and predicted (relative) depth maps using our trained VGG16 FCN8s [43, 42]. There is often a black blob around the center of the image, a singularity in depth estimation caused by the focus of expansion. (a)(b)(c): images from the CityDriving dataset, (d): image from the KITTI dataset, and (e): image from the CityScapes dataset.

profile, which stands out from the background. To excel at relative-depth estimation, the CNN will benefit by learning to recognize such structures.

The goal of our work is to show that pre-training a network to do depth prediction is a powerful *surrogate (proxy) task* for learning visual representations. In particular, we show that a network pre-trained for relative depth prediction is a powerful starting point from which to train a deep network for downstream tasks including semantic segmentation, joint semantic reasoning of road segmentation and car detection, and monocular (absolute) depth estimation. This regime allows us to obtain significant performance gains on urban scene understanding benchmarks such as KITTI [15, 14] and CityScapes [5], compared to training a segmentation model from scratch. In fact, our performance on semantic segmentation and joint semantic reasoning tasks comes very close to that of equivalent architectures pre-trained with ImageNet [6], a massive labeled dataset. Also, it performs better than other models with pre-training on other proxy tasks using unlabeled data. For the monocular depth estimation, our pre-trained model achieves better performance than an ImageNet pre-trained model.

One might assume that the more similar the domain of unlabeled visual data used for the proxy task (here, three urban scene understanding tasks) is to the domain in which the eventual semantic task is defined (here, semantic segmentation), the better the representation learned by pre-training. This observation allows us to go beyond simple pre-training, and effectively provides a *domain adaptation* mechanism. By adapting (fine-tuning) a relative depth prediction model to targets obtained from unlabeled data in a novel domain (say, driving in a new city) we can improve the underlying representation, priming it for better perfor-

mance on a semantic task (e.g., segmentation) trained with a small labeled dataset from this new domain. In experiments, we show that pre-training on unlabeled videos from a target city, absent any labeled data from that city, consistently improves all urban scene understanding tasks.

In total, our work advances two pathways for integrating unlabeled data with visual learning. First, we propose a novel proxy task for self-supervised learning of visual representations; it is based on learning to predict relative depth, inferred from unlabeled videos. This task offers competitive or better results (for monocular depth estimation) when used as a pre-training alternative to ImageNet classification. Second, we show that our task can be used to drive domain adaptation. Experiments demonstrate its utility in scene understanding tasks for street scenes in a novel city. Remarkably, our adapted model achieves results that are competitive with state-of-the-art method on the KITTI depth estimation benchmark. New methods, such as those we introduce, of extracting knowledge from unlabeled data are likely to be increasingly important as computer vision scales to real-world applications; here massive dataset size can outpace herculean annotation efforts.

2. Related Work

The idea of posing supervised prediction tasks on unlabeled data has been leveraged for both images and videos. The idea, often called self-supervision, is most typically realized by removing part of the input and then training a network to predict it. This can take the shape of deleting a spatial region and trying to inpaint it [37], draining an image of color and trying to colorize it [25, 53, 26], or removing the final frame in a sequence and trying to hallucinate it [39, 45, 31, 48, 52, 30]. Generative Adversarial Net-

works, used for inpainting and several future frame prediction methods, can also be used to generate realistic-looking samples from scratch. This has found secondary utility for unsupervised representation learning [38, 44, 10]. Another strategy is to extract patches and try to predict their spatial or temporal relationship. In images, this has been done for pairs of patches [7] or for 3-by-3 jigsaw puzzles [34]. In videos, it can be done by predicting the temporal ordering of frames [32, 27].

The correlation of frames in video is a rich source of self-supervised learning signals. The assumption that close-by frames are more similar than far apart frames can be used to train embeddings on pairs [33, 19, 21] or triplets [49] of frames. A related idea that the representation of interesting objects should change slowly through time dates back to Slow Feature Analysis [51].

There is also work on using multi-modal sensory input as a source of supervision. Owens *et al.* [35] predict statistics of ambient sounds in videos. A single-image depth predictor can be trained from raw stereo images, by warping the right image with a depth map predicted from the left image and train it to reconstruct the left image [13, 16]. This idea was extended in recent work to support fully self-supervised training on regular video, by predicting both depth and camera pose difference for pairs of nearby frames [55, 47]. Neither of these two works emphasizes more general-purpose feature learning. Jayaraman & Grauman [20] learn a representation equivariant to ego-motion transformations, using ideas from metric learning. Agrawal *et al.* [1] concurrently developed a similar method that uses the ego-motion directly as the prediction target as opposed to as input to an equivariant transformation. Both of these works assume knowledge of the agent’s own motor actions, which limits their evaluation in sample size due to lack of publicly available data. In our work, the ego-motion is inferred through optical flow, which means we can leverage large sources of crowd-sourced data, such as YouTube videos.

In a recent work, Pathak *et al.* [36] use optical flow and a graph-based algorithm to produce unsupervised segmentation maps. A network is then trained to approximate these maps, driving representation learning. The reliance on moving objects, as opposed to a moving agent, could make it harder to collect good data. Using a method based on ego-motion, the agent can promote its own representation learning simply by moving, instead of having to find objects that move. Beyond studying a single source of self-supervision, combining multiple self-supervision sources is increasingly popular. In [8], a set of self-supervision tasks are integrated via a multi-task setting. Wang *et al.* [50] propose to combine instance-level as well as category-level self-supervision. Both [8, 50] achieve better performance than a single model.

3. Learning from Relative Depth

As a surrogate task, our goal is to induce a feature representation $f(I)$ of an RGB image $I(x, y)$ by predicting its depth image $z(x, y)$, where the representation $f(I)$ could be transferred to other downstream tasks (*e.g.*, semantic segmentation) with fine-tuning. In section 3.1, we introduce technical details of gathering images and corresponding depth maps. In section 3.2, we provide details of training CNNs to learn the feature representation $f(I)$.

3.1. Self-Supervised Depth

As described above, we automatically produce depth images for video frames by analyzing the motion of pre-existing videos. In our experiments, we used three sets of videos: YouTube videos, videos from the KITTI database [15, 14], and videos from the CityScapes database [5]. The YouTube videos consist of 135 videos taken from moving cars in major U.S. cities². We call this dataset CityDriving. The stability of the camera in these videos makes them relatively easy for the depth estimation procedure. Some of the videos are extremely long, lasting several hours. The CityDriving dataset features a large number of man-made structures, pedestrians and cars. Following [28], we only keep two consecutive frames if they have moderate motion (*i.e.*, neither too slow nor too fast). To eliminate near duplicate frames, two consecutive depth maps must be at least 2 frames apart. We keep only the first one of two consecutive frames and the computed depth image. In total, we gathered 1.1M pairs of RGB images and their corresponding depth maps, where the typical resolution is 360×640 . Similarly, we collect 30K and 24K pairs of RGB images and their relative depth maps for CityScapes and KITTI, respectively.

To obtain the depth map of each frame from a video, we:

- compute the optical flow between a pair of frames [18];
- estimate the translational component of the optical flow and the direction of camera translation from the optical flow, using the method of [2];
- estimate the scene depth, up to an unknown scale factor, from the translational component of the optical flow and the camera direction estimate.

We now explain these steps in detail.

Denote the instantaneous coordinates of a point P in the environment by $(X, Y, Z)^T$, and the translational velocity of the camera in the environment by $(U, V, W)^T$. Let the motion field component (idealized optical flow) of the point P (in the image plane) be (u, v) , corresponding to the horizontal and vertical image motion, respectively. The motion

²They are crawled from a YouTube playlist, taking less than an hour.

field can be written as the sum of translation and rotation components³

$$u = u_t + u_r, \quad v = v_t + v_r, \quad (1)$$

where the subscript t and r denote translation and rotation, respectively. According to the geometry of perspective projection [17], the following equations hold if the motion of the camera is purely translational,

$$u_t = \frac{-U + xW}{Z}, \quad v_t = \frac{-V + yW}{Z}, \quad (2)$$

where x and y are the coordinates of the point P in the image plane (the origin is at the image center).

Note that the depth Z can be estimated from either one of these equations. However, the estimate can be unstable if either u_t or v_t is small. To obtain a more robust estimate of Z , we square the two equations above and add them:

$$Z = \sqrt{\frac{(-U + xW)^2 + (-V + yW)^2}{u_t^2 + v_t^2}}. \quad (3)$$

Because we can only recover $(U, V, W)^T$ up to scale (see below), we can only compute the depth map of an image up to scale. To induce feature representations, we use depth orderings of pixels in an image. We compute the relative depth $z \in [0, 1]$ of the pixel P as its depth percentile (divided by 100) across all estimated depth values for the image. Since these percentiles are invariant to the velocity’s unknown scale, we do not need to recover the absolute scale of velocity. Examples of these automatically obtained depth maps are given in Figure 1 and Figure 2.

To compute the optical flow, we use the state-of-the-art unsupervised method [18]. It first computes sparse pixel matchings between two video frames. It then interpolates to get dense pixel-wise optical flow fields from sparse matchings, where we replace the supervised edge detector [9] with its unsupervised version [28]. Based on the optical flow, we use the method proposed in [2] to recover the image motion of each pixel due to translational motion only (u_t, v_t) , and also, the global camera motion $(U, V, W)^T$ up to an unknown scale factor. We now briefly summarize [2].

The authors start with the observation that, for strictly translational camera motions (relative to the scene), there is a one-to-one mapping between the possible motion directions of the camera and the *angle part* of the motion field, which the authors call an *angle field*. This implies that if the rotational component of the motion field can be removed, the remaining motion field can be described with a (usually) small number of angle fields: one corresponding to the

³Any motion in the image is due to the relative motion of a world point and the camera. This addresses motion of either the object, the camera, or both.



Figure 2: Samples of image pairs and computed translational optical flow that we use to recover the relative depth. From left to right: first images, second images, translational optical flow between input two images, and relative depth of the first images.

background and one for each moving object in the scene. The authors show how the rotation of the camera can be estimated by finding the rotation such that the remaining motion can be well-explained by angle fields. This procedure produces a translational optical flow field (u_t, v_t) , and a set of regions in the image corresponding to the background and different object motions, along with the motion directions (U, V, W) of those regions. The depth value of each pixel can then be recovered according to Eq. 3. See [18, 2] for more details.

3.2. Predicting Depth From a Single Image

While a CNN for predicting depth from a single image is a core component of our system, we are primarily interested in depth prediction as a proxy task, rather than an end in itself. We therefore select standard CNN architectures and focus on quantifying the power of the depth task for pre-training and domain adaptation, compared to using the same networks with labeled data. Specifically, we work with variants of the standard AlexNet [23] and VGG16 [43] architectures.

Given an RGB image I , we need pixel-wise predictions in the form of a depth image z , so we modify both AlexNet and VGG16 to produce output with the same spatial resolution as the input image. In particular, we consider Fully Convolutional Networks (FCNs) [42] and U-Nets [16, 55]. Detailed discussions can be found in the experiment section.

Since the relative depth (*i.e.*, the depth percentile) is estimated over the entire image, it is essential to feed the entire image to the CNN to make a prediction. For CityDriving and KITTI, we simply resize the input image to 224×416 and 352×1212 . For CityScapes, we discard the bottom 20% portion of each video frame containing mainly the hood of a car, which remains static over all videos and makes the rel-

Table 1: Results of semantic segmentation using different architectures on different datasets. CD=CityDriving, CS=CityScapes, K=KITTI.

pre-training	FCN32s			FCN16s			FCN8s		
	CityScapes	CamVid	KITTI	CityScapes	CamVid	KITTI	CityScapes	CamVid	KITTI
ImageNet	58.7	63.7	51.5	62.9	65.9	55.3	63.4	67.0	56.4
scratch	45.4	41.0	32.4	51.3	44.1	33.1	51.6	44.3	34.2
Ours CD	55.0	57.8	45.6	57.6	59.0	47.7	59.8	60.3	48.6
Ours CD+K	56.0	58.5	46.0	56.9	58.8	48.2	58.9	60.1	49.0
Ours CD+CS	56.2	58.5	47.4	58.5	58.8	47.8	60.5	59.9	49.6

ative depth estimation inaccurate (recall our relative depth estimation is mainly based on motion information). The cropped input image is then resized to 384×992 . During training, we employ horizontal flipping and color jittering for data augmentation. Since depth serves as a proxy, rather than an end task, even though the relative depth estimation is not always correct, the network is able to tolerate some degree of noise as shown in [36]; we can then repurpose the network’s learned representation.

In all experiments, we use L_1 loss for each pixel when training for depth prediction, *i.e.*, we train networks to regress the relative depth values. Both AlexNet and VGG16 variants are trained for 30 epochs using the Adam optimizer [22] with momentum of $\beta_1 = 0.9, \beta_2 = 0.999$, and weight decay of 0.0005. The learning rate is 0.0001 and is held constant during the pre-training stage.

4. Experiments

We consider three urban scene understanding tasks: semantic segmentation, joint semantic reasoning consisting of road segmentation and object detection [46], and monocular depth estimation.

The experiments reported in this section are aimed at two goals. First, we investigate the effect, on various downstream tasks, of pre-training the representation (CNN) on the self-supervised relative depth prediction. Second, we evaluate pre-training on unlabeled videos from the test domain as a mechanism for adapting to domain shift.

4.1. Semantic Segmentation

We consider three datasets commonly used for evaluating semantic segmentation. Their main characteristics are summarized below:

KITTI [41]: 100 training images, 46 testing images, spatial dimensions of 370×1226 , 11 classes.

CamVid [4, 3]: 367 training images, 101 validation images, 233 testing images, spatial dimensions of 720×960 , 11 classes.

CityScapes [5]: 2975 training images, 500 validation images, 1525 testing images, spatial dimensions of $1024 \times$

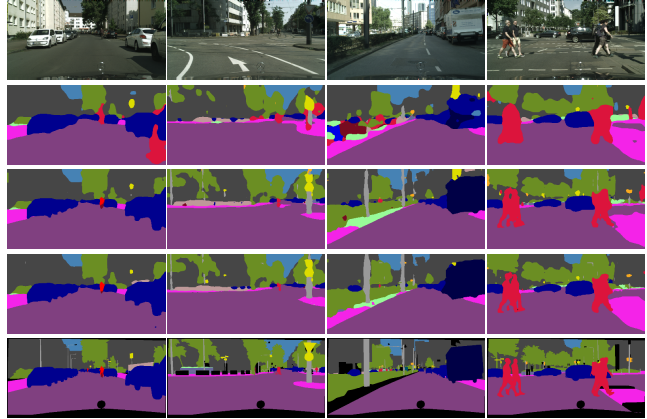


Figure 3: Qualitative results on CityScapes. From top to bottom: input images, FCN8s predictions no pre-training, our FCN8s predictions, ImageNet FCN8s predictions, and ground-truth annotations. The difference between the 2nd and 3rd rows shows a clear benefit of pre-training with depth prediction.

2048, 19 classes. We conduct experiments on images at half resolution.

The first two datasets are much too small to provide sufficient data for “from scratch” training of a deep model; CityScapes is larger, but we show below that all three datasets benefit from pre-training. We use the curated annotations of the CamVid dataset released by [24]. As a classical CNN-based model for semantic segmentation, we report results of different variants of the Fully Convolutional Network (FCN) [42]. Following [42], the FCNs are trained sequentially, *i.e.*, from FCN32s to FCN16s, and finally to FCN8s.⁴ Each one is used to initialize its successor. We compare variants of FCNs based on the VGG16 architecture [43] with no pre-training, an ImageNet pre-trained model, and our own pre-trained with relative depth data. We follow [42] and report the intersection over union (IoU) as evaluation metrics over all classes.

⁴32, 16, 8 are the downsampling factor of the top convolution layer. Generally, the smaller it is, the better the model performs as the predictions are less coarse with smaller downsampling factor.

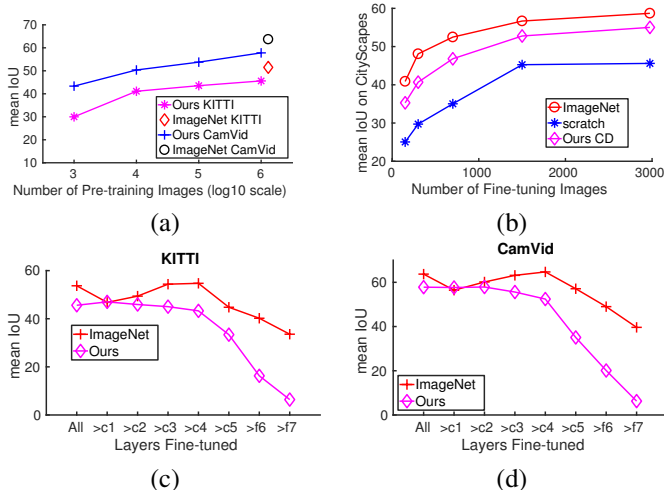


Figure 4: Ablation studies of performance by (a) varying number of pre-training images on Kitti and CamVid, (b) varying number of fine-tuning images of CityScapes, (c)(d) fine-tuning different layers of our depth and ImageNet pre-trained models on Kitti and CamVid, respectively.

During training, the inputs are random crops of 352×352 for Kitti and 704×704 for CamVid. Each FCN variant is trained for 600 epochs with a batch size of 16 using 4 GPUs. For CityScapes, to ease the computational burden, we use half-resolution input images. The inputs to the network are random crops of 512×512 . Each FCN variant is trained for 400 epochs with a batch size of 16. In addition to the random crops, random horizontal flips and color jittering are also performed. The CNNs at this stage (learning segmentation) are trained or fine-tuned using the Adam optimizer, where weight decay is 0.0005. For the learning rate, we use 0.0001 for FCN32s and decrease it by factor of 10 at the 400th epoch (300th epoch for CityScapes). For FCN16s and FCN8s, the learning rate is set to 0.00002 and 0.00001, respectively, and kept constant during training.

We report results of each variant on the testing set of Kitti and CamVid and validation set of CityScapes in Table 1. Detailed results for each category can be found in the supplementary material. First of all, we can see that each FCN variant benefits from our pre-trained model (“Ours CD” in Table 1), compared with no pre-training. Second, the models pre-trained on ImageNet outperform our counterpart.

4.2. Ablation Studies

We perform ablation studies using VGG16 FCN32s on the semantic segmentation datasets. Specifically, we study the following aspects.

Number of pre-training images. Figure 4(a) demonstrates that the performance of our depth pre-trained model scales

Table 2: Results of joint semantic reasoning, including road segmentation and car detection.

pre-training	Road Segmentation		Car Detection (AP)		
	F_1	AP	Easy	Medium	Hard
ImageNet	96.33	92.26	95.59	86.43	72.28
scratch	93.78	91.37	89.37	79.93	66.02
Ours CD	94.74	92.13	92.84	84.73	69.47
Ours CD+K	95.66	92.14	94.31	85.72	70.50

linearly with the log of the number of pre-training images on CamVid, which is similar to the conclusion of [36].

On Kitti, our pre-trained model initially has a big performance boost when the number of pre-training images increases from 1K to 10K. With enough data (more than 10K), the performance also scales linearly with the log of the number of the pre-training images.

Number of fine-tuning images. Figure 4(b) shows that every model (ImageNet, scratch, our depth pre-trained model) benefits from more fine-tuning data on the CityScapes dataset. For both ImageNet and our depth pre-trained models, it suggests that more fine-tuning data is also beneficial for transferring the previously learned representations to a new task.

Fine-tuning different layers. Figure 4(c)(d) demonstrate the results of fine-tuning some layers and fixing the rest on the downstream datasets, Kitti and CamVid, respectively. It is interesting to note that fixing the first two convolution layers (>c1 and >c2) of an ImageNet pre-trained VGG16 harms the performance. In contrast, it does not affect the performance of our pre-trained model much. In fact, our model can get slightly better results by fixing the first convolution layer than by fine-tuning it, both on Kitti and CamVid, suggesting that the lowest-level features of our model are more suitable for urban scene segmentation (recall that our model is pre-trained on the CityDriving dataset). On the other hand, we also notice that the performance of both ImageNet and our own pre-trained models drop significantly by fine-tuning the last three layers (>c5, >f6, and >f7) only. But the performance of our model drops more quickly, suggesting that features in the top layers (c5, f6, and f7) of an ImageNet pre-trained VGG16 generalize better than ours.

4.3. Other tasks

Joint Semantic Reasoning. Joint semantic reasoning is important for urban scene understanding, especially with respect to tasks such as autonomous driving [46]. We investigate the effectiveness of our pre-trained model using the MultiNet architecture [46] for joint road segmentation

Table 3: Monocular depth estimation on the KITTI dataset using the split of Eigen *et al.* [11]. For model details, Arch.=Architecture, #Inf. indicates number of inference passes through a model, A=AlexNet, V=VGG16, and R=ResNet50. For training data, Class.=classification, I=ImageNet, CD=CityDriving, K=KITTI, CS=CityScapes. (*Both [16] and [55] use a VGG16-like architecture.)

Method	Model Details		Training Data				Error Metrics				Accuracy Metrics		
	Arch.	#Inf.	Class.	Stereo	Video	GT Depth	Abs Rel	Sq Rel	RMSE	RMSE log	$\delta < 1.25$	$\delta < 1.25^2$	$\delta < 1.25^3$
Eigen <i>et al.</i> [11]	A	1	I	-	-	K	0.203	1.548	6.307	0.282	0.702	0.890	0.958
Liu <i>et al.</i> [29]	A	1	I	-	-	K	0.202	1.614	6.523	0.275	0.678	0.895	0.965
Godard <i>et al.</i> [16]	V*	1	-	K	-	-	0.148	1.344	5.927	0.247	0.803	0.922	0.964
Godard <i>et al.</i> [16]	V*	1	-	CS+K	-	-	0.124	1.076	5.311	0.219	0.847	0.942	0.973
Godard <i>et al.</i> [16]+pp	V*	2	-	CS+K	-	-	0.118	0.923	5.015	0.210	0.854	0.947	0.976
Godard <i>et al.</i> [16]+pp	R	2	-	CS+K	-	-	0.114	0.898	4.935	0.206	0.861	0.949	0.976
Zhou <i>et al.</i> [55]	V*	1	-	-	K	-	0.208	1.768	6.856	0.283	0.678	0.885	0.954
Zhou <i>et al.</i> [55]	V*	1	-	-	CS+K	-	0.198	1.836	6.565	0.275	0.718	0.901	0.960
Ours	V	1	I	-	-	K	0.143	0.970	5.250	0.217	0.797	0.935	0.979
Ours	V	1	-	-	-	K	0.150	1.085	5.475	0.232	0.774	0.921	0.972
Ours	V	1	-	-	CD	K	0.137	0.931	5.028	0.209	0.807	0.941	0.981
Ours	V	1	-	-	CD+K	K	0.131	0.881	4.862	0.203	0.822	0.944	0.981

and car detection.⁵ MultiNet consists of a single encoder, using the VGG16 as backbone, and two sibling decoders for each task. For road segmentation, the decoder contains three upsampling layers, forming an FCN8s. The car detection decoder directly regresses the coordinates of objects. Following [46], the entire network is jointly trained using the Adam optimizer, using a learning rate of 0.00005 and weight decay of 0.0005 for 200K steps. We refer readers to [46] for more technical details.

We replace the ImageNet-trained VGG16 network with a randomly initialized one and our own VGG16 pre-trained on CityDriving using relative depth. For the road segmentation task, there are 241 training and 48 validation images. For car detection, there are 7K training images 481 validation images. Detailed comparisons on the validation set can be found in Table 2. We use the F_1 measure and Average Precision (AP) scores for road segmentation evaluation and AP scores for car detection. AP scores for different car categories are reported separately. We can clearly see that our pre-trained model (Ours CD) consistently outperforms the randomly initialized model (scratch in Table 2) but is still worse than the ImageNet pre-trained model as with semantic segmentation.

Monocular Depth Estimation. For the monocular depth estimation, we adopt the U-Net architecture [40] similar to [16, 55], which consists of a fully convolutional encoder and another fully convolutional decoder with skip connections. In order to use an ImageNet pre-trained model, we replace the encoder with the VGG16 architecture. We use the training and validation set of [16], containing 22.6K

and 888 images, respectively. We evaluate our model on the Eigen split [11, 16], consisting of 697 images, where ground-truth absolute depth values are captured using LiDAR at sparse pixels. Unlike [16], which uses stereo image pairs as supervision to train the network, or [55], which uses neighboring video frames as supervision to train the network (yet camera intrinsic parameters are required), we use the absolute sparse LiDAR depth values to fine-tune our network. The entire network is trained for 300 epochs using the Adam optimizer with a weight decay of 0.0005. The initial learning rate is 0.0001 and decreased by factor of 10 at the 200th epoch.

Detailed comparisons can be found in Table 3. We have two observations. First, our network using the ImageNet pre-trained VGG16 outperforms previous methods, except that it is slightly worse than [16] trained on CityScapes and KITTI stereo image pairs. Compared with [11, 29], we use a deeper ImageNet pre-trained model (VGG16 versus AlexNet). Compared to other unsupervised methods, since we use ground-truth depth values, it is reasonable to expect our model to achieve better results. Second, our depth pre-trained model outperforms both the ImageNet counterpart and a randomly initialized model. This is perhaps due to the alignment between the pre-training task, relative depth estimation, and the downstream task, absolute depth estimation.

4.4. Domain Adaptation by Pre-Training

In the experiments described above, the two stages (pre-training on self-supervised depth prediction, followed by supervised training for segmentation) rely on data that come from significantly different domains. The self-supervised learning uses videos obtained from moving in North America. In contrast, none of the target dataset images were

⁵We use the author’s released code <https://github.com/MarvinTeichmann/MultiNet>. As the scene classification data is not publicly available, we only study road segmentation and car detection here.

collected in the same geographic locations. For instance, CityScapes includes data from driving in German cities. Thus, in addition to a shift in task, the fine-tuning of the network for segmentation must also deal with a *domain shift* in the input.

CityScapes [5] and KITTI [15] make available video sequences that give temporal context to every image in the dataset. None of these extra frames are labeled, but we can leverage them in the following way. Before training the network on segmentation, we fine-tune it, using the same self-supervised relative depth prediction task described in Section 3.1, on these videos. Our intuition is that this may induce some of the modifications in the network that reflect the changing distribution of the input. Then, we proceed as before to train the fine-tuned representation on the semantic segmentation data, keeping hyperparameters of this training stage the same as in previous experiments. Specifically, we fine-tune our pre-trained model on the CityDriving dataset on CityScapes and KITTI, respectively.

For the semantic segmentation task, the last two rows of Table 1 demonstrate that such fine-tuning can consistently improve the performance of a self-supervised model over all FCN variants on both CityScapes and KITTI, validating its effectiveness as a domain adaptation approach. Interestingly, we can see that while fine-tuning is helpful for FCN32s on CamVid initially, it does not help much for FCN16s and FCN8s. Perhaps this is due to the domain gap between CamVid and CityScapes/KITTI.

For the joint semantic reasoning, using the domain adaptation strategy via fine-tuning on the KITTI raw videos, we can further close the gap between an ImageNet pre-trained model. Remarkably, after fine-tuning, the F_1 score of road segmentation and AP scores for easy and medium categories of our pre-trained model are pretty close to the ImageNet counterpart’s. (See last row of Table 2.)

Similarly, for the monocular depth estimation, pre-training as domain adaptation also improves the performance of our pre-trained model. After fine-tuning our pre-trained model using KITTI’s raw videos, our model achieves results that are competitive with state-of-the-art method [16].

In summary, our domain adaptation by pre-training strategy consistently improves the performance of our pre-trained model over all urban scene understanding tasks.

4.5. Comparison with other Self-Supervised Models

Finally, we compare our results to those obtained with other self-supervision strategies surveyed in Section 2. All the results are obtained with FCN32s using the AlexNet architecture.⁶ We obtain new state-of-the-art results on all three urban scene segmentation datasets among meth-

⁶We were unable to get meaningful results with [37] on KITTI and with [20] on all three segmentation datasets.

Table 4: Comparisons of self-supervised models using AlexNet FCN32s. CS=CityScapes, K=KITTI, CV=CamVid.

pre-training method	supervision source	CS	K	CV
supervised	ImageNet labels	48.1	46.2	57.4
none	-	40.7	39.6	44.0
tracking [49]	motion	41.9	42.1	50.5
moving [1]	ego-motion	41.3	40.9	49.7
watch-move [36]	motion seg.	41.5	40.8	51.7
frame-order [32]	motion	41.5	39.7	49.6
context [37]	appearance	39.7	-	37.8
object-centric [12]	appearance	39.6	39.1	48.0
colorization [25, 26]	appearance (color)	42.9	35.8	53.2
cross-channel [54]	misc.	36.8	40.8	46.3
audio [35]	video soundtrack	39.6	40.7	51.5
Ours (depth)	depth	45.4	42.6	53.4

ods that use self-supervised pre-training. In particular, our model outperforms all other self-supervised models with motion cues (the first four self-supervised models in Table 4). Moreover, our pre-trained model performs significantly better than the model learned from scratch on all three datasets, validating the effectiveness of our pre-training.

5. Conclusions

We have proposed a new proxy task for self-supervised learning of visual representations. It requires only access to unlabeled videos taken by a moving camera. Representations are learned by optimizing prediction of relative depth, recovered from estimated motion flow, from individual (single) frames. Although ostensibly non-semantic, training for this task is likely to encourage emergence of semantically meaningful representations, since scene understanding can provide significant cues for predicting depth. Indeed, we show this task to be a powerful proxy task, which is competitive with recently proposed alternatives as a means of pre-training representations on unlabeled data. We also demonstrate a novel application of such pre-training, aimed at domain adaptation. When given videos taken by cars driven in cities, self-supervised pre-training primes the downstream urban scene understanding networks, leading to improved accuracy after fine-tuning on a small amount of manually labeled data.

Our work offers novel insights about one of the most important questions in vision today: how can we leverage unlabeled data, and in particular massive amounts of unlabeled video, to improve recognition systems. While a comprehensive picture of self-supervision methods and the role they play in this pursuit is yet to emerge, our results suggest that learning to predict depth is an important piece of this pic-

ture.

Acknowledgement

The experiments were performed using equipment obtained under a grant from the Collaborative R&D Fund managed by the Massachusetts Tech Collaborative.

References

- [1] P. Agrawal, J. Carreira, and J. Malik. Learning to see by moving. In *CVPR*, pages 37–45, 2015. 3, 8
- [2] P. Bideau and E. Learned-Miller. It’s moving! A probabilistic model for causal motion segmentation in moving camera videos. In *ECCV*, 2016. 3, 4
- [3] G. J. Brostow, J. Fauqueur, and R. Cipolla. Semantic object classes in video: A high-definition ground truth database. *Pattern Recognition Letters*, 2008. 5, 10
- [4] G. J. Brostow, J. Shotton, J. Fauqueur, and R. Cipolla. Segmentation and recognition using structure from motion point clouds. In *ECCV*, pages 44–57, 2008. 5, 10
- [5] M. Cordts, M. Omran, S. Ramos, T. Rehfeld, M. Enzweiler, R. Benenson, U. Franke, S. Roth, and B. Schiele. The cityscapes dataset for semantic urban scene understanding. In *CVPR*, 2016. 2, 3, 5, 8, 10
- [6] J. Deng, W. Dong, R. Socher, L.-J. Li, K. Li, and L. Fei-Fei. ImageNet: A large-scale hierarchical image database. *CVPR*, 2009. 2
- [7] C. Doersch, A. Gupta, and A. A. Efros. Unsupervised visual representation learning by context prediction. In *ICCV*, pages 1422–1430, 2015. 3
- [8] C. Doersch and A. Zisserman. Multi-task self-supervised visual learning. In *ICCV*, 2017. 3
- [9] P. Dollár and C. L. Zitnick. Fast edge detection using structured forests. *IEEE Trans. Pattern Anal. Mach. Intell.*, 37(8):1558–1570, 2015. 4
- [10] J. Donahue, P. Krähenbühl, and T. Darrell. Adversarial feature learning. In *ICLR*, 2017. 3
- [11] D. Eigen, C. Puhrsch, and R. Fergus. Depth map prediction from a single image using a multi-scale deep network. In *NIPS*, pages 2366–2374, 2014. 7
- [12] R. Gao, D. Jayaraman, and K. Grauman. Object-centric representation learning from unlabeled videos. In *ACCV*, pages 248–263, 2016. 8
- [13] R. Garg, B. G. V. Kumar, G. Carneiro, and I. D. Reid. Unsupervised CNN for single view depth estimation: Geometry to the rescue. In *ECCV*, pages 740–756, 2016. 3
- [14] A. Geiger, P. Lenz, C. Stiller, and R. Urtasun. Vision meets robotics: The KITTI dataset. *International Journal of Robotics Research (IJRR)*, 2013. 2, 3
- [15] A. Geiger, P. Lenz, and R. Urtasun. Are we ready for autonomous driving? the KITTI vision benchmark suite. In *CVPR*, 2012. 2, 3, 8
- [16] C. Godard, O. Mac Aodha, and G. J. Brostow. Unsupervised monocular depth estimation with left-right consistency. In *CVPR*, 2017. 3, 4, 7, 8
- [17] B. K. P. Horn. *Robot Vision*. MIT Press, Cambridge, MA, USA, 1986. 4
- [18] Y. Hu, Y. Li, and R. Song. Robust interpolation of correspondences for large displacement optical flow. In *CVPR*, 2017. 3, 4
- [19] P. Isola, D. Zoran, D. Krishnan, and E. H. Adelson. Learning visual groups from co-occurrences in space and time. *arXiv preprint arXiv:1511.06811*, 2015. 3
- [20] D. Jayaraman and K. Grauman. Learning image representations tied to ego-motion. In *ICCV*, pages 1413–1421, 2015. 3, 8
- [21] D. Jayaraman and K. Grauman. Slow and steady feature analysis: higher order temporal coherence in video. In *CVPR*, 2016. 3
- [22] D. P. Kingma and J. Ba. Adam: A method for stochastic optimization. In *ICLR*, 2015. 5
- [23] A. Krizhevsky, I. Sutskever, and G. E. Hinton. Imagenet classification with deep convolutional neural networks. In *NIPS*, pages 1106–1114, 2012. 4
- [24] A. Kundu, V. Vineet, and V. Koltun. Feature space optimization for semantic video segmentation. In *CVPR*, pages 3168–3175, 2016. 5
- [25] G. Larsson, M. Maire, and G. Shakhnarovich. Learning representations for automatic colorization. In *ECCV*, 2016. 2, 8
- [26] G. Larsson, M. Maire, and G. Shakhnarovich. Colorization as a proxy task for visual understanding. In *CVPR*, 2017. 2, 8
- [27] H. Lee, J. Huang, M. Singh, and M. Yang. Unsupervised representation learning by sorting sequences. In *ICCV*, 2017. 3
- [28] Y. Li, M. Paluri, J. M. Rehg, and P. Dollár. Unsupervised learning of edges. In *CVPR*, pages 1619–1627, 2016. 3, 4
- [29] F. Liu, C. Shen, G. Lin, and I. D. Reid. Learning depth from single monocular images using deep convolutional neural fields. *IEEE TPAMI.*, 38(10):2024–2039, 2016. 7
- [30] W. Lotter, G. Kreiman, and D. Cox. Deep predictive coding networks for video prediction and unsupervised learning. In *ICLR*, 2017. 2
- [31] M. Mathieu, C. Couprie, and Y. LeCun. Deep multi-scale video prediction beyond mean square error. *arXiv preprint arXiv:1511.05440*, 2015. 2
- [32] I. Misra, C. L. Zitnick, and M. Hebert. Unsupervised learning using sequential verification for action recognition. 2016. 3, 8
- [33] H. Mobahi, R. Collobert, and J. Weston. Deep learning from temporal coherence in video. In *ICML*, 2009. 3
- [34] M. Noroozi and P. Favaro. Unsupervised learning of visual representations by solving jigsaw puzzles. In *ECCV*, 2016. 3
- [35] A. Owens, J. Wu, J. H. McDermott, W. T. Freeman, and A. Torralba. Ambient sound provides supervision for visual learning. In *ECCV*, 2016. 3, 8
- [36] D. Pathak, R. B. Girshick, P. Dollár, T. Darrell, and B. Hariharan. Learning features by watching objects move. In *CVPR*, 2017. 3, 5, 6, 8
- [37] D. Pathak, P. Krähenbühl, J. Donahue, T. Darrell, and A. Efros. Context encoders: Feature learning by inpainting. In *CVPR*, 2016. 2, 8

- [38] A. Radford, L. Metz, and S. Chintala. Unsupervised representation learning with deep convolutional generative adversarial networks. 2016. 3
- [39] M. Ranzato, A. Szlam, J. Bruna, M. Mathieu, R. Collobert, and S. Chopra. Video (language) modeling: a baseline for generative models of natural videos. *arXiv preprint arXiv:1412.6604*, 2014. 2
- [40] O. Ronneberger, P. Fischer, and T. Brox. U-net: Convolutional networks for biomedical image segmentation. In *MIC-CAI*, pages 234–241, 2015. 7
- [41] G. Ros, S. Ramos, M. Granados, A. Bakhtiary, D. Vázquez, and A. M. López. Vision-based offline-online perception paradigm for autonomous driving. In *WACV*, 2015. 5, 10
- [42] E. Shelhamer, J. Long, and T. Darrell. Fully convolutional networks for semantic segmentation. *TPAMI*, 2017. 2, 4, 5, 10
- [43] K. Simonyan and A. Zisserman. Very deep convolutional networks for large-scale image recognition. *CoRR*, abs/1409.1556, 2014. 2, 4, 5
- [44] J. T. Springenberg. Unsupervised and semi-supervised learning with categorical generative adversarial networks. In *ICLR*, 2016. 3
- [45] N. Srivastava, E. Mansimov, and R. Salakhutdinov. Unsupervised learning of video representations using lstms. In *ICML*, 2015. 2
- [46] M. Teichmann, M. Weber, J. M. Zöllner, R. Cipolla, and R. Urtasun. Multinet: Real-time joint semantic reasoning for autonomous driving. In *CVPR*, 2016. 5, 6, 7
- [47] S. Vijayanarasimhan, S. Ricco, C. Schmid, R. Sukthankar, and K. Fragkiadaki. Sfm-net: Learning of structure and motion from video. In *CVPR*, 2017. 3
- [48] C. Vondrick, H. Pirsaviash, and A. Torralba. Generating videos with scene dynamics. In *NIPS*, pages 613–621, 2016. 2
- [49] X. Wang and A. Gupta. Unsupervised learning of visual representations using videos. In *ICCV*, 2015. 3, 8
- [50] X. Wang, K. He, and A. Gupta. Transitive invariance for self-supervised visual representation learning. In *ICCV*, 2017. 3
- [51] L. Wiskott and T. J. Sejnowski. Slow feature analysis: Unsupervised learning of invariances. *Neural computation*, 14(4):715–770, 2002. 3
- [52] T. Xue, J. Wu, K. Bouman, and B. Freeman. Visual dynamics: Probabilistic future frame synthesis via cross convolutional networks. In *NIPS*, pages 91–99, 2016. 2
- [53] R. Zhang, P. Isola, and A. A. Efros. Colorful image colorization. In *ECCV*, 2016. 2
- [54] R. Zhang, P. Isola, and A. A. Efros. Split-brain autoencoders: Unsupervised learning by cross-channel prediction. In *CVPR*, 2017. 8
- [55] T. Zhou, M. Brown, N. Snavely, and D. G. Lowe. Unsupervised learning of depth and ego-motion from video. In *CVPR*, 2017. 3, 4, 7

Appendix A. Semantic Segmentation

The IoU scores of each FCN8s [42] with different pre-training models on CityScapes [5], KITTI [41], and CamVid [4, 3] datasets are shown in Table 5, Table 6, and Table 7, respectively.

Appendix B. More Visual Results

For car detection on the KITTI dataset, the visual results are shown in Figure 5.

For road segmentation on the KITTI dataset, the visual results are shown in Figure 6.

For monocular depth results on the KITTI dataset, the visual results are shown in Figure 7.

	Road	Sidewalk	Building	Wall	Fence	Pole	Light	Sign	Vegetation	Terrain	Sky	Person	Rider	Car	Truck	Bus	Train	Motorbike	Bike	mIoU
ImageNet	96.6	75.8	88.4	45.7	45.3	33.3	48.0	56.5	87.8	56.5	90.2	65.3	42.1	88.9	49.9	69.3	54.3	47.1	63.5	63.4
scratch	95.4	68.5	84.7	30.0	36.6	20.1	29.7	44.7	86.8	48.5	86.5	52.8	33.3	83.6	28.3	50.5	27.7	19.0	53.2	51.6
Ours CD	96.5	74.8	87.7	39.1	39.7	39.2	42.8	55.5	88.7	53.4	91.4	63.4	37.3	88.8	38.2	57.1	45.1	35.9	61.7	59.8
Ours CD+K	96.4	73.0	86.7	31.8	35.7	36.8	40.9	52.9	88.1	49.9	90.8	62.5	36.4	88.6	40.5	60.4	48.7	37.1	61.1	58.9
Ours CD+CS	96.6	75.3	87.7	38.3	41.1	38.3	44.0	54.9	88.9	54.2	91.3	63.2	36.4	89.0	43.0	61.8	47.1	35.4	62.0	60.5

Table 5: Comparisons of different FCN8s on the CityScapes dataset. Top to bottom: ImageNet pre-trained model, no pre-training (train the model on KITTI from scratch), our pre-trained models on the CityDriving dataset, our pre-trained model on CityDriving and then fine-tuned on KITTI, and our pre-trained model on CityDriving and then fine-tuned on CityScapes. For abbreviations: CD=CityDriving, CS=CityScapes, and K=KITTI.

Method	Bldng	Tree	Sky	Car	Sign	Road	Pedest.	Fence	Pole	Sidewk.	Bicycle	mn. IoU
ImageNet	85.3	79.7	85.5	81.7	26.0	93.0	9.8	39.9	30.0	75.2	14.2	56.4
scratch	68.6	72.7	78.5	48.2	12.2	45.9	0.0	6.1	18.6	25.0	0.0	34.2
Ours CD	81.5	76.7	84.3	67.5	17.0	84.2	0.04	31.6	24.5	63.3	3.9	48.6
Ours CD+K	81.5	77.2	84.4	69.4	18.0	81.4	0.2	34.9	31.4	60.0	0.2	49.0
Ours CD+CS	83.0	75.9	84.5	72.2	17.8	85.4	1.5	33.5	26.6	64.2	1.3	49.6

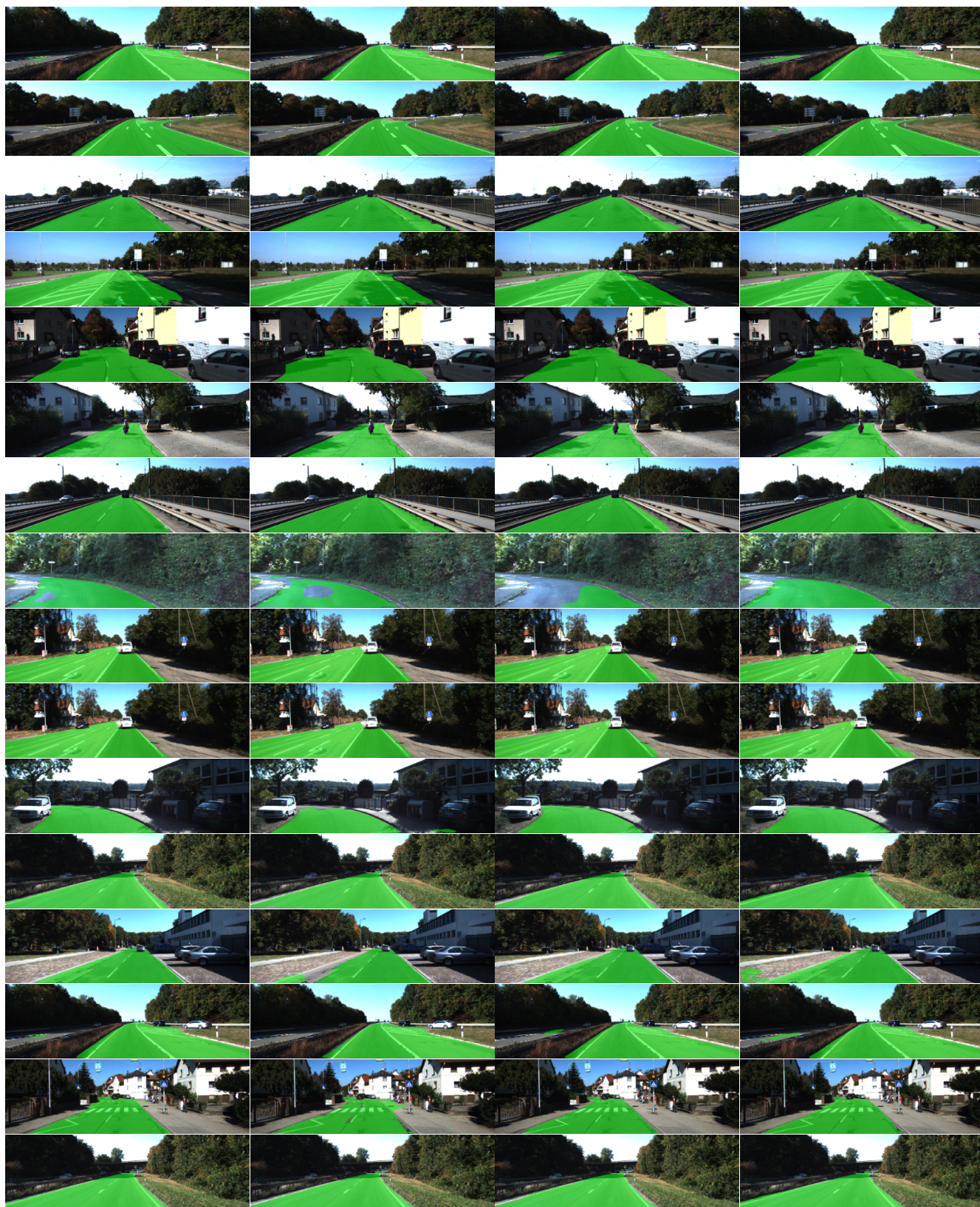
Table 6: Comparisons of different FCN8s on the KITTI dataset. Top to bottom: ImageNet pre-trained model, no pre-training (train the model on KITTI from scratch), our pre-trained models on the CityDriving dataset, our pre-trained model on CityDriving and then fine-tuned on KITTI, and our pre-trained model on CityDriving and then fine-tuned on CityScapes. For abbreviations: CD=CityDriving, CS=CityScapes, and K=KITTI.

Method	Building	Tree	Sky	Car	Sign	Road	Pedestrian	Fence	Pole	Sidewalk	Bicycle	mean IoU
ImageNet	77.9	93.1	84.5	37.1	25.4	90.9	78.4	47.4	58.8	83.7	60.0	67.0
scratch	61.4	82.4	71.0	19.9	11.7	87.4	46.7	5.7	25.2	54.7	21.4	44.3
Ours CD	73.9	90.4	80.0	27.1	23.4	90.1	68.8	40.8	47.7	77.6	43.6	60.3
Ours CD+K	73.9	89.5	80.2	27.1	25.2	90.3	66.5	41.2	48.0	75.7	43.5	60.1
Ours CD+CS	74.3	89.7	80.2	25.0	23.0	90.2	67.1	39.5	48.9	77.2	43.6	59.9

Table 7: Comparisons of different FCN8s on the CamVid dataset. Top to bottom: ImageNet pre-trained model, no pre-training (train the model on KITTI from scratch), our pre-trained models on the CityDriving dataset, our pre-trained model on CityDriving and then fine-tuned on KITTI, and our pre-trained model on CityDriving and then fine-tuned on CityScapes. For abbreviations: CD=CityDriving, CS=CityScapes, and K=KITTI.



Figure 5: Car detection results on the KITTI dataset. For abbreviations: CD=CityDriving and K=KITTI.



(a) ImageNet

(b) scratch

(c) Ours CD

(d) Ours CD+K

Figure 6: Road segmentation results on the KITTI dataset. For abbreviations: CD=CityDriving and K=KITTI.



Figure 7: Monocular depth estimation on the KITTI dataset. For abbreviations: CD=CityDriving, CS=CityScapes, and K=KITTI. The sparse ground-truth depth, capture using LiDAR, are interpolated for visualization purpose. Since only the bottom part has ground-truth depth values, only corresponding bottom part images are demonstrated here.